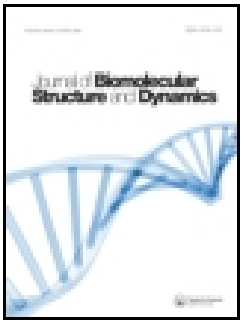

Journal of Biomolecular Structure and Dynamics

ISSN: (Print) (Online) Journal homepage: https://www.tandfonline.com/loi/tbsd20

Observing reorientation dynamics with Time-Resolved fluorescence and molecular dynamics in varying periodic boundary conditions

Gouri S. Jas, Ed W. Childs, C. Russell Middaugh & Krzysztof Kuczera

To cite this article: Gouri S. Jas, Ed W. Childs, C. Russell Middaugh & Krzysztof Kuczera (2021): Observing reorientation dynamics with Time-Resolved fluorescence and molecular dynamics in varying periodic boundary conditions, Journal of Biomolecular Structure and Dynamics, DOI: 10.1080/07391102.2021.1947894

To link to this article: https://doi.org/10.1080/07391102.2021.1947894

JOURNAL OF BIOMOLECULAR STRUCTURE AND DYNAMICS
https://doi.org/10.1080/07391102.2021.1947894

Observing reorientation dynamics with Time-Resolved fluorescence and molecular dynamics in varying periodic boundary conditions

Gouri S. Jas[a], Ed W. Childs[b], C. Russell Middaugh[a] and Krzysztof Kuczera[c]

[a]Department of Pharmaceutical Chemistry, The University of Kansas, Lawrence, KS, USA; [b]Department of Surgery, Morehouse School of Medicine, Atlanta, GA, USA; [c]Department of Chemistry and Department of Molecular Biosciences, The University of Kansas, Lawrence, KS, USA

Communicated by Ramaswamy H. Sarma

ABSTRACT

This work presents a combined study of time-resolved fluorescence spectroscopy and all-atom molecular dynamics simulation to investigate periodic boundary conditions' and water models' influence on the orientation dynamics and translational and rotational diffusion of peptides in solution. We have characterized the effects of solvent box size and water model choice on the dynamics of two peptide systems, NATA and WK5. Computationally, translational, and rotational diffusion and internal fluctuations are investigated through all-atom molecular dynamics simulation with two water models and different box sizes. These results are compared with time-resolved fluorescence anisotropy decay (FAD) measurements. The associated time constant and orientation dynamics from FAD measurement along the ^1L_b axis provided baseline data to validate molecular dynamics simulation. The modeling results show that diffusion rates vary roughly in inverse proportion to water model viscosity, as one would expect. Corrections for finite box size are significant for translational diffusion and insignificant for rotational diffusion. This study also finds that internal dynamics described by autocorrelation functions and kinetic network models are relatively insensitive to both box size and water model properties. Our observation suggests that different peptide properties respond differently to a change in simulation conditions.

ARTICLE HISTORY
Received 23 April 2021
Accepted 17 June 2021

KEYWORDS
Time-resolved fluorescence; molecular dynamics simulations; periodic boundary conditions; kinetics; optimum dimensionality reduction

Introduction

The conformational motion of peptides and proteins in biological systems often accounts for their regulation capabilities and function. An extensive effort, applying theory and experiments, has been dedicated to probing internal motions, especially in the picosecond to microsecond time scale (Shoup & Szabo, 1982; Northrup et al., 1984; Morelli & Ten Wolde, 2008; Klein & Schwarz, 2014; Ilie et al., 2014; Berne & Pecora, 2000; Woessner, 1962a; Woessner, 1962b; Lipari & Szabo, 1982; Tjandra et al., 1995; Brüschweiler et al., 1995; Lee et al., 1997; Ghose et al., 2001; Wang et al., 1997; Boisbouvier et al., 2003; Duchardt et al., 2008; Wolf et al., 2012; Debye, 1929; Perrin, 1936; Perrin, 1934; Ortega et al., 2011; McKinney et al., 2003; Boisbouvier et al., 2003). Fluorescence spectroscopy with site-directed fluorophore has become an essential tool to study the dynamics and interactions of biomolecules (Lakowicz, 1999; Schröder et al., 2005; Loman et al., 2010; Hummer & Szabo, 2017; Szabo, 1980; Schuler et al., 2002; Margittai et al., 2003; Weiss, 1999; Schröder & Grubmüller, 2003; Munro et al., 1979; Jas et al., 2021; Jas et al., 2016). Since the fluorophore is attached to the peptide and protein system, time-resolved fluorescence anisotropy can be used to monitor structure, conformational changes, and flexibility in the system. Molecular dynamics simulation has become an essential computational tool for studying dynamic properties in a native-like environment and accurately interpreting experimental observation (Juszczak et al., 1997; Hasimoto, 1959; Dünweg & Kremer, 1993; Yeh & Hummer, 2004; Vögele & Hummer, 2016; Venable et al., 2017). A recent molecular dynamics study of rotational motion of horse heart myoglobin and B-DNA suggests effect from solvent box size on translational and rotational diffusion because of the introduction of periodic boundary conditions (PBC) (Linke et al., 2018). Here, in contrast to the previous study, we wanted to examine the finite-size effect on the reorientation dynamics on slightly smaller biomolecular systems by varying PBC using solvated systems with increasing simulation box size. Additionally, we have explored the difference in peptide dynamics upon solvation with TIP4P and TIP4P-EW water models, which differ significantly in viscosity.

Here we present a combined time-resolved fluorescence spectroscopic study and molecular dynamics simulation of two distinctly different peptide systems in solution. We have used solvated N-acetyl-Tryptophan-Amide (NATA) and a five-

CONTACT Gouri S. Jas gouri.jas@physicianscientists.org Department of Pharmaceutical Chemistry, The University of Kansas, Lawrence, KS, 66047, USA
Supplemental data for this article can be accessed online at https://doi.org/10.1080/07391102.2021.1947894.

residue peptide with tryptophan in the N-terminal and lysine in the C-terminal end and three alanine in between (WK5) for the measurements and the simulations. The N and C termini of WK5 were protected with acetylation and amidation, respectively. We have measured time-resolved fluorescence anisotropy targeting the tryptophan at several temperatures in the experimental component. Molecular dynamics simulation studies have been carried out on identical peptide systems to validate simulation and gain atomically detailed insight into experimental measurements. In the first part of two components MD studies, we examined the peptide motions using three different simulation boxes with the TIP4P water model. We examined and compared the dynamics of systems in three simulation box sizes and under two water models, TIP4P and TIP4P-EW. This carefully designed MD study is in place to monitor the influence of PBC and water model on the re-orientational dynamics and validate computational observation by comparing them with the time-resolved measurements.

This study's primary objective is to obtain microscopic information about the anisotropy experiments with an atomically detailed interpretation of the measured data. We specifically addressed the following questions:

How do the time-resolved fluorescence anisotropy decay measurements of the peptide system vary with increasing complexity from the simplest dipeptide to a five-residue peptide? How does a change in temperature affects the anisotropy decay? What can be inferred about the conformational dynamics from the anisotropy decay curve? How does a variation in the periodic boundary condition under a constant water model influence the reorientation dynamics? Is there a finite-size effect under a specific periodic boundary condition? A finite-size dependence of the rotational diffusion constant is assumed to be present under periodic boundary conditions. This combined, carefully designed study will test the validity of this assumption.

Methods

Materials

Experimental measurements on NATA and WK5 were performed by dissolving them in 20 mM acetate buffer of pH 4.8. The NATA was purchased from Sigma. The WK5 ($AcWA_3K\text{-}NH_2$) was obtained from GenScript Corporation with greater than 95% purity. Sample concentration for each peptide is determined with the absorbance of tryptophan at 280 nm with a molar extinction coefficient of 5690 $M^{-1}\,cm^{-1}$.

Circular dichroism

Far-UV circular dichroism spectroscopy for both NATA and WK5 at pH 4.8 are measured with a JASCO 815 spectropolarimeter in a cylindrical cell with a path length of 0.5 mm and at a concentration of ~120 μM concentration. The recorded spectral range of CD spectra is between 170 − 260 nm.

Fluorescence anisotropy decay measurements

The experimental setup of the time-resolved fluorescence spectroscopy is described in detail elsewhere. Briefly, NATA and WK5 fluorescence is generated with excitation at 290 nm wavelength of light. Fluorescence was collected at 350 nm with an 8-nm bandpass monochromator. Similarly, parallel and perpendicular fluorescence polarizations are collected simultaneously in a T-format. Rotational correlation times for the NATA and WK5 were obtained by globally fitting the fluorescence decays with polarization parallel and perpendicular to the excitation polarization.

Computational

The influence of varying solvent box size and solvent viscosity on the structure and dynamics of NATA and WK5 were analyzed from all-atom MD simulation trajectories in explicit solvent. We generated four explicit solvents MD trajectories of 200 ns length for NATA. Three trajectories were generated with the TIP4P water model in a cubic box of 32.9 Å, 41.7 Å, and 47.9 Å, respectively. Additionally, a single trajectory was generated with TIP4P-EW water in a 32.9 Å cubic box. Analogously, four MD trajectories of 5,000 ns length were generated for WK5. Three trajectories were with TIP4P (Jorgensen & Jenson, 1998) water model and cubic box sizes of 40.4 Å, 50.3 Å, and 56.2 Å, respectively, and a single trajectory with TIP4P-EW (Horn et al., 2004) water and a cubic box size of 40.4 Å. The trajectories with the largest box sizes have been described elsewhere (Jas et al., 2016), while the TIP4P-EW trajectories were described in more detail elsewhere (Jas et al., 2021). The three box sizes are further denoted as PBC1, PBC2, and PBC3, for brevity. System details are summarized in Tables S1 and S2 of the SI. Initial peptide structures were generated with CHARMM (Brooks et al., 2009) in the extended conformation for NATA and helical form for WK5. Solvation, the addition of ions, energy minimization, NPT equilibration at 1 bar and 300 K, and NVT trajectory generation at 300 K were performed with GROMACS version 4.5.6 and 5.1.4 (Hess et al., 2008); the OPLS-AA protein force field (Kaminski & Jorgensen, 1996). The PME (Li et al., 2013) method was used to describe long-range electrostatic interactions, van der Waals interactions were truncated at 1.0 nm, and all bonds were constrained with LINCS (Heinz et al., 2001).

In simulations, the ionization states of titratable groups have been assigned at pH 7, i.e. with a protonated Lys sidechain in the WK5 pentapeptide and all remaining groups neutral. These same ionization states are also appropriate at the experimental conditions of pH 4.5, as pK_a values for all groups present lie well outside the 4.5-7.0 pH range.

Autocorrelation functions (ACFs) were calculated for selected system variables to describe system dynamics. For distance-type variables x, we use $C_1(t) = \langle \Delta x(t))\Delta x(0)\rangle$, with $\Delta x(t) = x(t) - \langle x\rangle$, while for angle-type variables ϕ, we use the circular statistics result from $C_1(t) = \langle \cos(\phi - \langle\phi\rangle)\rangle$, with $\langle\phi\rangle$ defined as in Jammalamadaka et al. Correlation times were obtained from these ACFs in two ways. Most simply, an average correlation time was generated by integration from

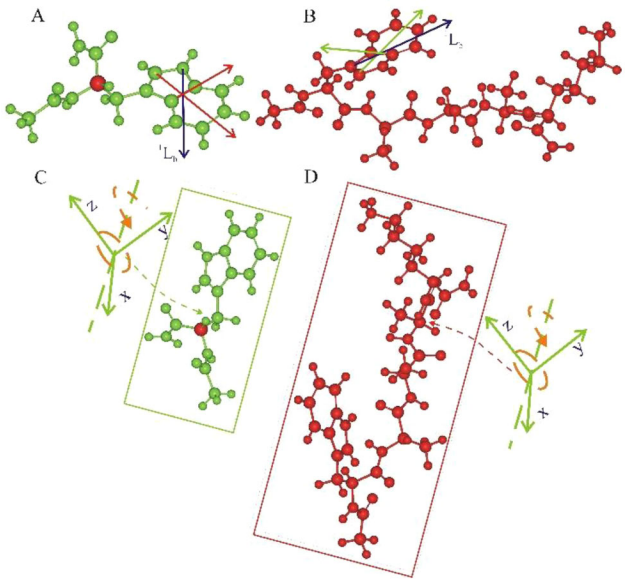

Figure 1. Axis systems for peptide reorientation. (A) LOC system on Trp side-chain in NATA. Axes a and b are shown in red, ^1L_b axis representing the transition dipole in black. (B) LOC system for WK5. Axes a and b are shown in green, ^1L_b axis in black. (C) CM system for NATA, axes in the green, center-of-mass location indicated with a dashed arrow (close to CB atom) shown at $t = 0$. (D) CM system for WK5, axes in the green, center-of-mass location indicated with a dashed arrow (close to ALA4 CB) shown at $t = 0$.

$t = 0$ to $t = t_c$, where the cutoff time is defined by $C(t_c) = 0.01$. Alternatively, the functions were fitted to sums of two exponentials.

Raw values of translational diffusion coefficients D_{tr} were calculated from mean-squared-displacements of molecular centers-of-mass using GROMACS (Hess et al., 2008). PBC corrections D_{tr} were considered as described by In-Chul et al. (Yeh & Hummer, 2004)

Rotational diffusion coefficients D_{rot} were calculated in two ways. In the first, local approach (further denoted as LOC), three orthogonal axes were defined for the indole side chain of Trp in NATA and WK5: axis *a* between CD2 and CE2 atoms, axis *b* between atom CD1 and center of CH2 and CZ3, and axis *c* defined as the vector product of *a* and *b* (Figure 1A and B). In the second global approach (further denoted as CM or center-of-mass), the axes were defined by eigenvectors of the peptide instantaneous moment of inertia tensor in the trajectories. Here axes *x1*, *x2*, and *x3* corresponded to the largest, intermediate, and lowest eigenvalues, respectively (Figure 1C and D). In both methods, autocorrelation functions $C_1(t) = \langle \cos(\theta) \rangle$ for reorientations of each of the three axes were calculated, with θ the axis reorientation during time t. Time constants from integrals of the functions, as described above, were used to calculate the rotational diffusion coefficients D_{rot}. Complete details are described in SI. PBC corrections for D_{rot} were applied following Linke et al. (Linke et al., 2018)

To model observed rotational correlation times corresponding to experimentally observed FAD signals, $C_2(t) = \langle 3\cos^2(\theta) - 1 \rangle$ functions were calculated, where θ is the reorientation during time t for the ^1L_b transition dipole axis of tryptophan. The ^1L_b axis orientation is obtained as a combination of *a* and *b* indole in-plane vectors according to the description in Yamamoto et al. (Yamamoto & Tanaka, 1972) (Figure 1A and B).

A synthetic description of peptide conformational dynamics was generated by building kinetic network models using the Optimal Dimensionality Reduction (ODR) (Hummer & Szabo, 2015), and Markov State Modeling (MSM) (Bowman et al., 2014) approaches. Details of these procedures have been described elsewhere. Briefly, discretization of state space is performed by dihedral angle clustering, and a set of transitions between microstates is generated based on MD trajectories. These are used to obtain the kinetic matrix **K** in ODR and transition matrix **T** in MSM. In ODR, the PCCA+ (Kube & Weber, 2007) is employed for kinetic coarse-graining, and the optimal reduced rate matrix **R** is obtained (Hummer & Szabo, 2015). MSM models are generated with Emma 1.4 (Senne et al., 2012). More details on the kinetic models are given in the SI.

Experimental results

Axis representation

Two-axis systems were employed to analyze molecular reorientations, the local LOC system on the tryptophan and the global CM system on the center of mass, as described in the Computational methods (Figure 1). The decay times measured in time-resolved fluorescence anisotropy experiments were compared with results from two-exponential fits to computed $C_2(t)$ ACFs of ^1L_b, transition dipole. Time constants associated with the C2(t) ACF of 1Lb and CM-X2 are in good agreement with the experimental time constants.

Circular dichroism

Far-UV circular dichroism (CD) spectra of NATA and the pentapeptide WK5 at pH 4.8 as a function of temperature between 266 K and 333 K are measured, analyze, and details are reported elsewhere (Jas et al., 2019). To specify the studied system's structural properties, here we have shown the far-UV CD spectrum at 293 K for both NATA and WK5 in Figure 2A and 2B, respectively. Figure 2C and D show the starting structure of NATA and WK5, respectively, from molecular modeling studies. Figure 2A shows the CD spectrum of NATA at 293 K with two minima at 210 and 198 nm and two maxima at 225 and 185 nm, suggesting the presence of ordered structural population in the CD at 293 K. In Figure 2B is the CD spectrum of WK5 at 293 K. There are two maxima at 227 and 185 nm and a minimum at 198 nm for WK5. There was also an appreciable amplitude at 220 nm. These three components suggest the presence of distinct populations of three secondary structural elements.

Fluorescence anisotropy decay

Tryptophan fluorescence decay in parallel and perpendicular polarization are shown in Figures 3 and 4. NATA fluorescence decays for parallel and perpendicular polarization at 283 K

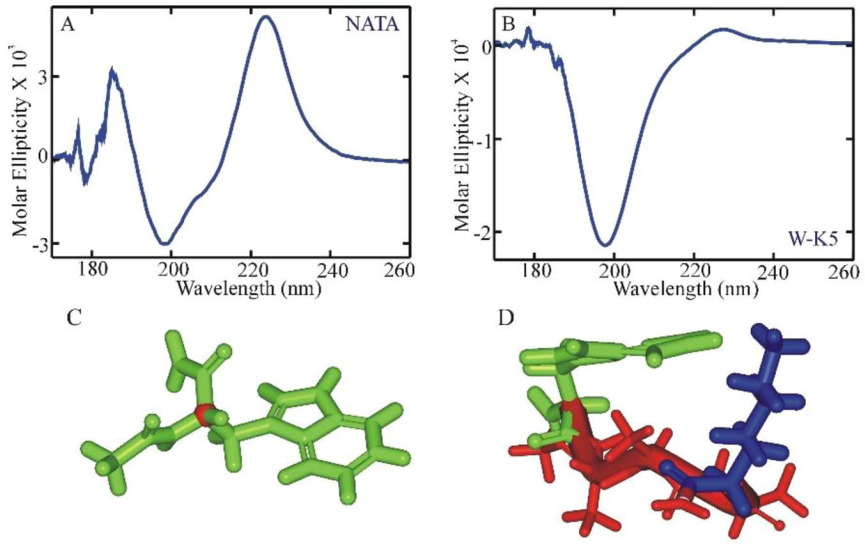

Figure 2. Far-UV circular dichroism measurements at 303 K for NATA (2 A) and WK5 (2B). Starting structures employed in molecular dynamics simulation for NATA (2 C) and WK5 (2 D).

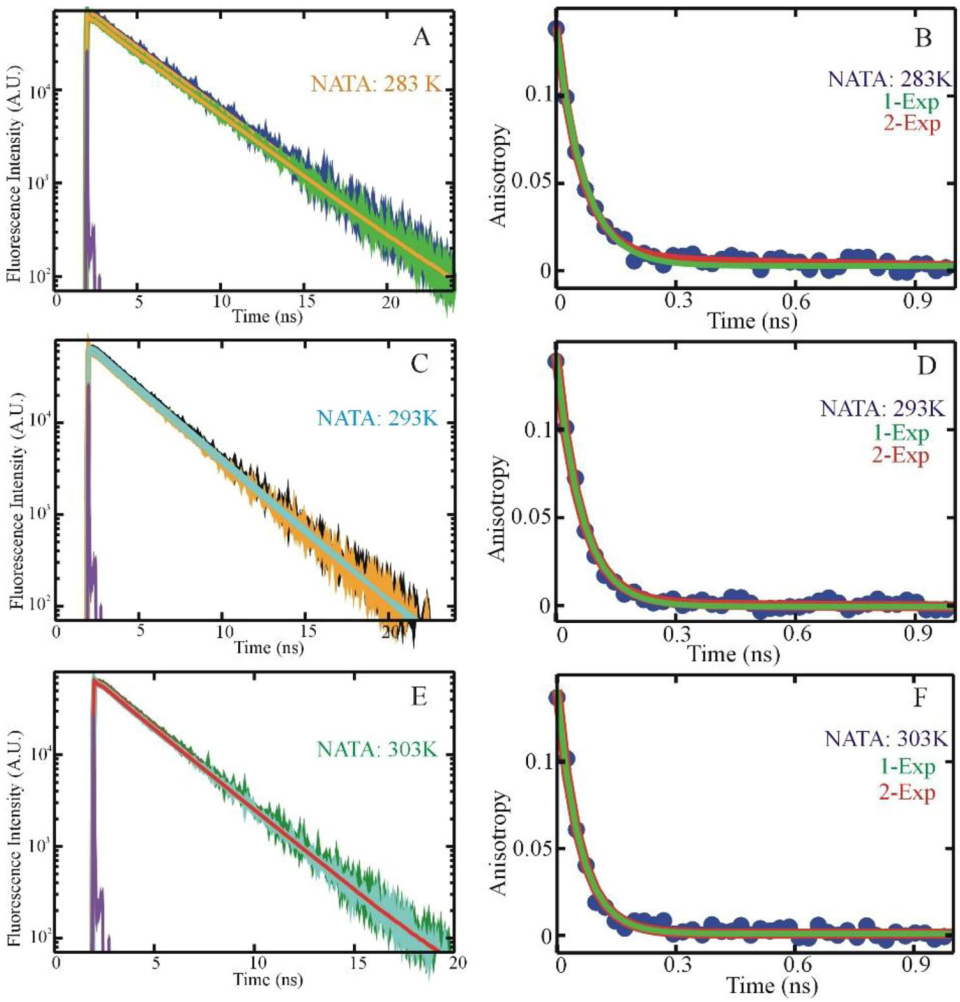

Figure 3. Time-resolved fluorescence in the parallel and perpendicular polarization with a sum of two exponential fit and instrument function (light blue) for NATA at 283 K (blue-parallel, green-perpendicular, orange-fit), 293 K (dark-blue-parallel, orange-perpendicular, cyan-fit), and 303 K (green-parallel, cyan-perpendicular, red-fit) are shown in 3 A, 3 C, and 3E. Fluorescence anisotropy decay (blue) for NATA at 283 K, 293 K, and 303 K are with a single exponential (green), and a sum of two exponential fits (red) are shown in 3B, 3 D, and 3 F.

(blue and green), 293 K (blue and orange), and 303 K (green and cyan) in acetate buffer at pH 4.8 are presented in Figure 3A, C, and E, respectively.

Fluorescence decays for parallel and perpendicular polarization for WK5 at 283 K (blue and green), 293 K (red and green), and 303 K (green and cyan) in acetate buffer at

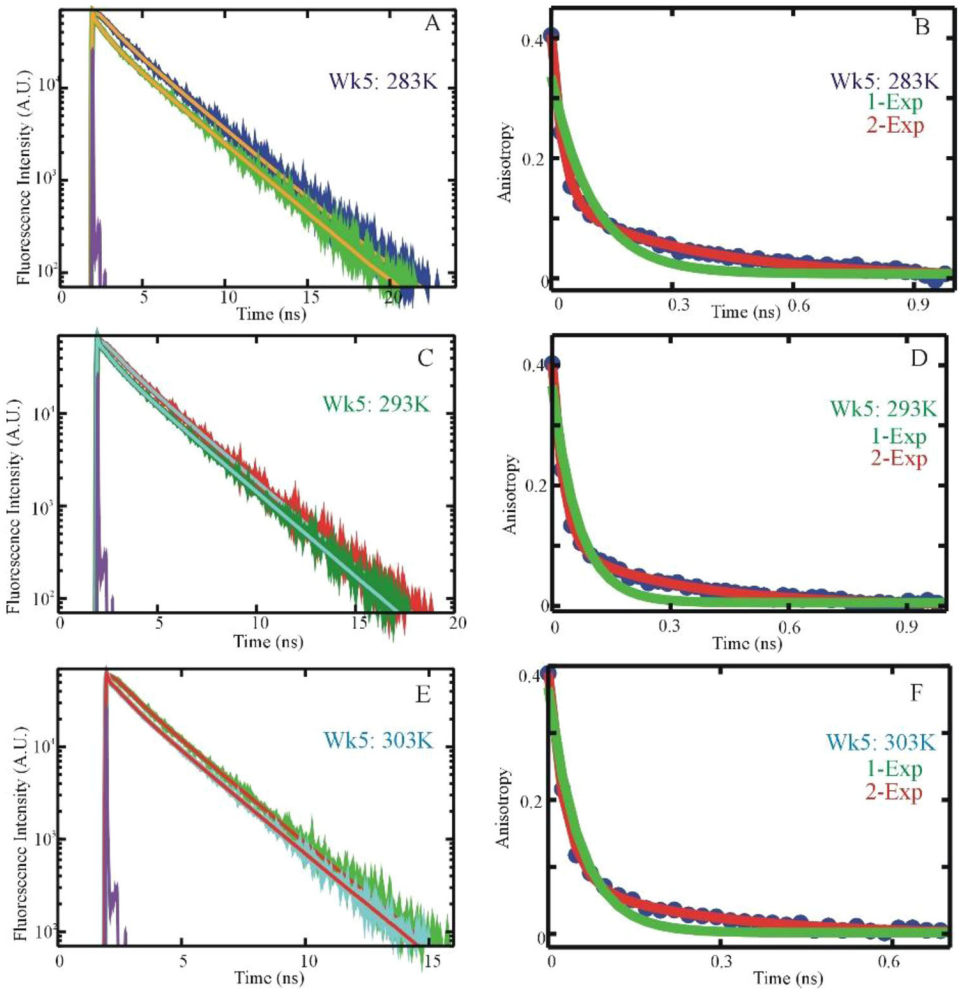

Figure 4. WK5 time-resolved fluorescence in the parallel and perpendicular polarization with a sum of two exponential fit and instrument function (light blue) at 283 K (blue-parallel, green-perpendicular, orange-fit), 293 K (red-parallel, dark-green-perpendicular, cyan-fit), and 303 K (light-green-parallel, cyan-perpendicular, red-fit) are shown in 4 A, 4 C, and 4E. Fluorescence anisotropy decay (blue) at 283 K, 293 K, and 303 K with a single exponential (green) and a sum of two exponential fits (red) are shown in 4B, 4 D, and 4 F.

pH 4.8 are presented in Figure 4A, C, and E, respectively. A bi-exponential fit to each data set is shown with the solid line.

Fluorescence anisotropy decay (blue) with a single (green) and bi-exponential (red) fits all data at 283 K, 293 K, and 303 K of NATA and Wk5 are shown in Figures 3B, D, F, and 4B, D, F, respectively. A bi-exponential fit with two-time constants at each temperature for NATA is 6.2ps and 94 ps at 283 K, 6 ps and 83ps at 293 K, and 5.5ps and 60ps 303 K, respectively.

This analysis suggests that the longer reorientation time is getting significantly faster with increasing temperature. The faster time constants are nearly temperature independent. One of the possible reasons for this observation may be a coupled motion where reorientational motion moves through the initiation and propagation pathway. Time constants associated with a bi-exponential fit to the anisotropy decay of WK5 at 283 K, 293 K, and 303 K are 29ps and 328ps, 28ps 298ps, and 26ps and 247ps, respectively. The faster time constants for WK5 in a nearly temperature independent manner, as seen in NATA.

When each anisotropy decay curve was fitted with a single exponential function, shown in green with each decay curve (blue), it could not fully describe the complete data set. Whereas a bi-exponential function adequately describes the entire curve, indicating the measured decay is a bi-exponential process.

A possible explanation for this observation may be a motion combining two distinct processes involving initiation and global motions within the measured reorientation dynamics in NATA and WK5. Here the initial step is an initiation process in the form of an internal motion through vibration and translation. It may then propagate to trigger a global reorientational motion. The initiation process starts with the vibrational motion upon excitation of the tryptophan indole ring with 280 nm photons which eventually propagates and manifests into a global movement. It appears that the initiation process is nearly temperature independent in the measured temperature range between 283 K and 303 K. The slower components of NATA are measured to be about three times faster than WK5. These findings point to size differences in an identical solution. This is a reasonable assessment considering the smaller hydrodynamics volume and compactness of NATA.

Overall, fluorescence anisotropy decay and far-UV circular dichroism spectroscopy for NATA and WK5 presented a

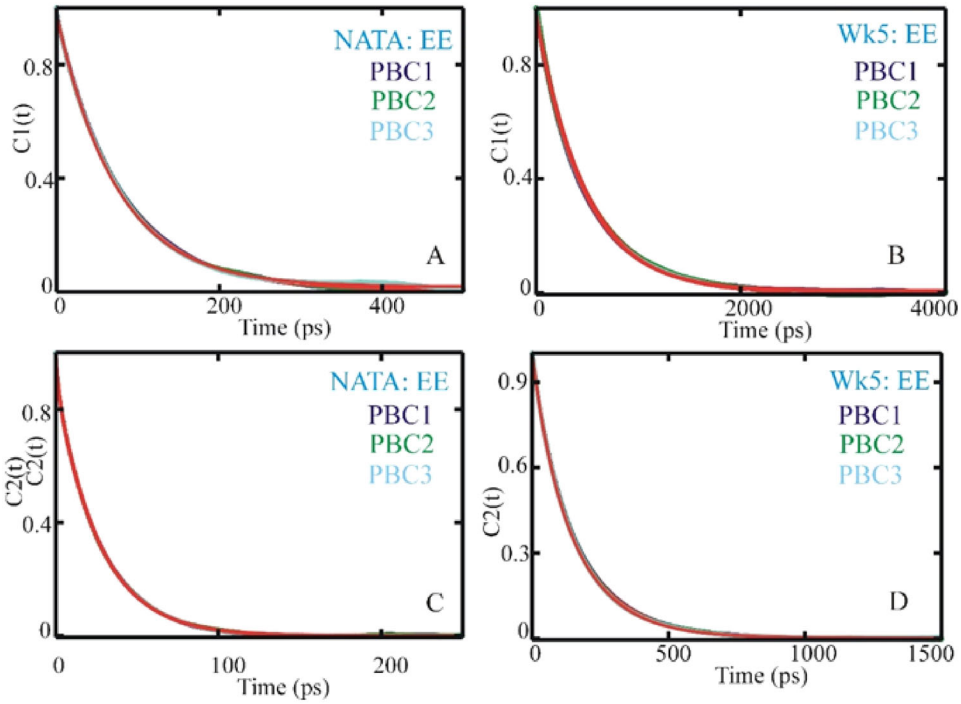

Figure 5. Examples of $C_1(t)$ and $C_2(t)$ ACFs for fluctuations of the end-to-end distance coordinate following MD trajectory of NATA (5 A, 5 C) and WK5 (5B, 5 D) at 300 K with TIP4P in PBC1, PBC2, and PBC3. ACFs are in blue, green, and light blue. A sum of two exponential fits to the ACFs are in red.

consistent insight for structural and dynamical behavior in solution. Structurally, MEF analysis showed that even in the simplest peptide, NATA could have two sets of identifiable populations with a discernable lifetime. CD analysis showed they could be a distorted and extended helix. Combining these two experiments can characterize the heterogeneous population of structures in solution and assign them with a lifetime. WK5 derived two dominant species, like poly-L-proline II and beta-hairpin, with a significantly less populated α-helical population. Analysis of the fluorescence lifetime data (Jas et al., 2019) suggests that NATA and WK5 adopt two different shapes in an identical solvent environment. Time-resolved fluorescence anisotropy decay of NATA and WK5 showed two very different reorientation times under identical temperature and solvent conditions. The reorientation time for WK5 is slower by a factor of about three compared to NATA. These results illustrate a significant difference in these two peptide systems' shape and size in an identical solution condition, with WK5 being larger than NATA.

To obtain anatomically detailed insight and an accurate interpretation of these experimental measurements and validate computational results, we have carried out all-atom molecular dynamics (MD) simulation of NATA and WK5 by varying periodic boundary conditions and water models.

Molecular dynamics results

We have performed MD simulations to characterize internal motions, translational and orientation dynamics, and associated diffusion coefficients of the peptides in solution. A detailed description of NATA and WK5 structure and dynamics from MD trajectories have been presented elsewhere (Jas et al., 2021; Jas et al., 2016). Here we have focused on the effects of water models and solvent box sizes on MD simulation. We have generated MD trajectories with three different simulation box sizes and the TIP4P (Jorgensen & Jenson, 1998) water model for each peptide and one trajectory involving TIP4P-EW (Horn et al., 2004). Simulation details are given in Methods and SI. The three trajectories with varying box sizes and TIP4P water are considered to investigate the effects of simulation system size on peptide structure and dynamics. Trajectories with the same box size and different water models (TIP4P (Jorgensen & Jenson, 1998) and TIP4P-EW (Horn et al., 2004)) are employed to study the effects of water properties on peptide behavior. Initial structures of the peptides are given in Figures 2C and D. To analyze the internal dynamics of the peptides, we have calculated autocorrelation functions (ACFs) $C_1(t)$ and $C_2(t)$ for a range of variables, including end-to-end distance, hydrogen-bond length, the radius of gyration, root mean square deviation of the backbone C-alpha atoms (RMSD) and solvent accessible surface area. ACFs of the fluctuations of the end-to-end distance for NATA and WK5 are shown in Figure 5. The ACFs for NATA for in PBC1, PBC2, and PBC3 with TIP4P, Figures 5A and C, are nearly superimposed on one another. $C_1(t)$ and $C_2(t)$ correlations for WK5 in Figures 5B and D showed no significant deviation in PBC1, PBC2, PBC3 with the TIP4P (Jorgensen & Jenson, 1998) water model. Hydrogen bond fluctuation (HB) ACFs for NATA (Figure 6A) and WK5 in (Figure 6B) showed nearly identical behavior, as described in Figure 5 for NATA and WK5, with no significant deviations. ACFs considering other coordinate systems are shown in Figures 7 and 8 with corresponding probability

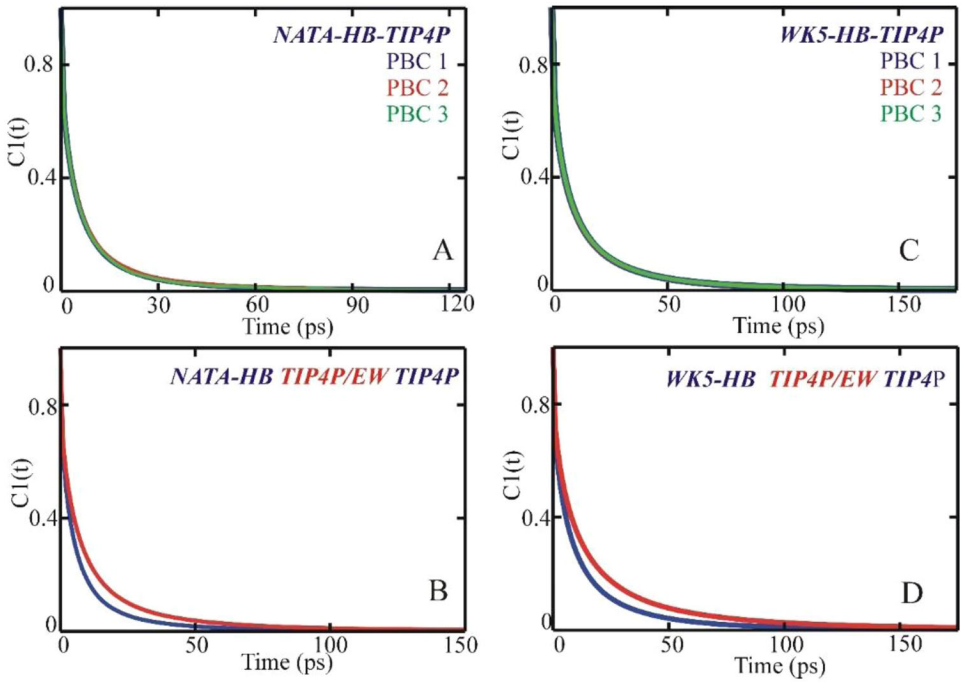

Figure 6. ACFs $C_1(t)$ for length fluctuations of hydrogen bonds – blocking acetyl CO with blocking amide NH_2 for NATA and acetyl C = O with peptide HN of LYS5 in WK5. (A) Different box sizes PBC1, PBC2, and PBC3 with TIP4P for NATA. (B) PBC1 box with TIP4P and TIP4P-EW for NATA. (C) Different box sizes PBC1, PBC2, and PBC3 with TIP4P for WK5. (D) PBC1 box with TIP4P and TIP4P-EW for WK5.

distributions. In all cases, there are no significant changes in behavior in varying simulation box sizes.

Figures 6 and 8 compare the ACFs for internal fluctuations for the TIP4P and TIP4P-EW (Horn et al., 2004) water models, with the box size kept constant for each peptide.

Comparison of HB $C_1(t)$ ACFs between TIP4P and TIP4P-EW showed slight deviations for both peptides (Figure 6C and D) with calculated correlation times agreeing within statistical errors. Effects of water model on SASA fluctuations were negligible (Figures 8C and D). Thus, for both NATA and WK5, it appears that the change from TIP4P to TIP4P-EW does not markedly influence the rates of internal fluctuations. Correlation times for several properties are given in the SI.

Anisotropy decay

The time constants (τ_2) associated with the $C_2(t)$ ACF for the indole ^1L_b axis may be compared with experimentally measured anisotropy decay times to establish the MD simulations' validity. To better represent the τ_2 data, the longer time constants from two-exponential fits to ^1L_b axis $C_2(t)$ obtained from the MD trajectories were employed, shown in Figures 9A and B. For NATA, the times are 33, 31, and 31 ps in the TIP4P trajectories and 44 ps in TIP4P-EW (Figure 9A, statistical errors are about 3 ps). For WK5, the times are 109, 110, and 96 ps in TIP4P and 158 ps in TIP4P-EW (Figure 9B, errors are about 6 ps). Thus, we find that the box size does not systematically influence τ_2. A Change of the water model does have a significant influence. The τ_2 times are ~40% slower for NATA and ~50% for WK5 in the more viscous TIP4P-EW. This is consistent with the viscosity change from 0.494 for TIP4P to 0.742 mPa s for TIP4P-EW at 298 K and 1 bar (Horn et al., 2004). Compared to the experimental data, 60 ps for NATA and 247 ps for WK5, the computed ^1L_b τ_2 time constant tend to be underestimated. This is consistent with our previous analysis (Jas et al., 2019).

Global vs. Local peptide reorientation

We have obtained two measures of molecular reorientation. The LOC axes' reorientations, located on the tryptophan indole group, follow the motions of this rigid sidechain and may be probed with FAD measurements. Reorientations of the CM axes describe changes in the moment of inertia tensor, which are sensitive to both the whole molecule's rotations and changes in the peptide shape. The x1 axis in the CM system, by definition, describes the slowest reorientations, while x2 and x3 are comparatively faster. As shown in Figure 10, the time scales of the CM-x1 axis reorientation do not vary systematically with box size for either peptide. The effect of the water model on CM-x1 reorientation is similar to that seen for the LOC ^1L_b axis, with ~50% change for NATA (Figure 10B) and ~30% for WK5 (Figure 10D) considering TIP4P and TIP4P-EW.

Interestingly, the CM-x1 reorientations are systematically slower than we found for LOC axes for the same simulation system, according to the intuition that the whole system should tend to move more slowly than its parts. However, the CM-x2 and x3 axes tend to reorient faster than the Trp-based LOC axes. This most probably is the result of more substantial effects of peptide shape change. Figure 9

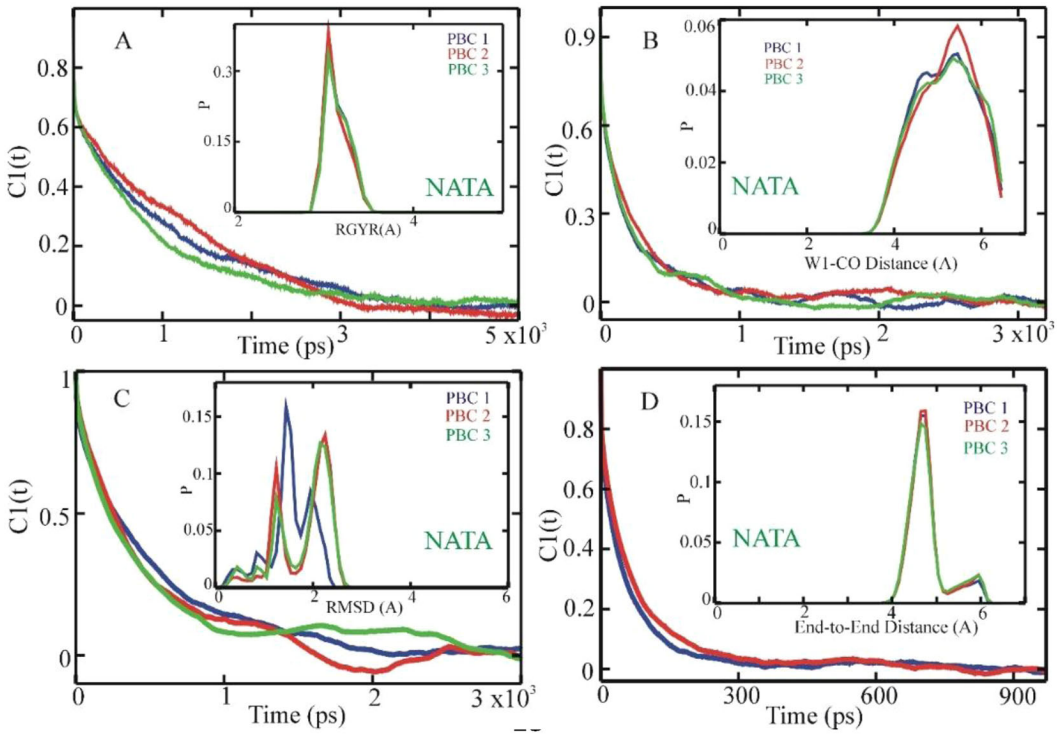

Figure 7. Examples of ACFs $C_1(t)$ for structural variables of NATA for three box sizes, PBC1, PBC2, and PBC at TIP4P water. (A) The radius of gyration (RGYR) (B) Acetyl blocking group carbonyl O distance from Trp sidechain (W1-CO) (C) non-hydrogen atom RMSD from starting structure (D) End-to-end distance (EE). Insets show probability distributions of the variables. Variation in RMSD value distributions reflects slight differences in starting structures after equilibration under the different conditions.

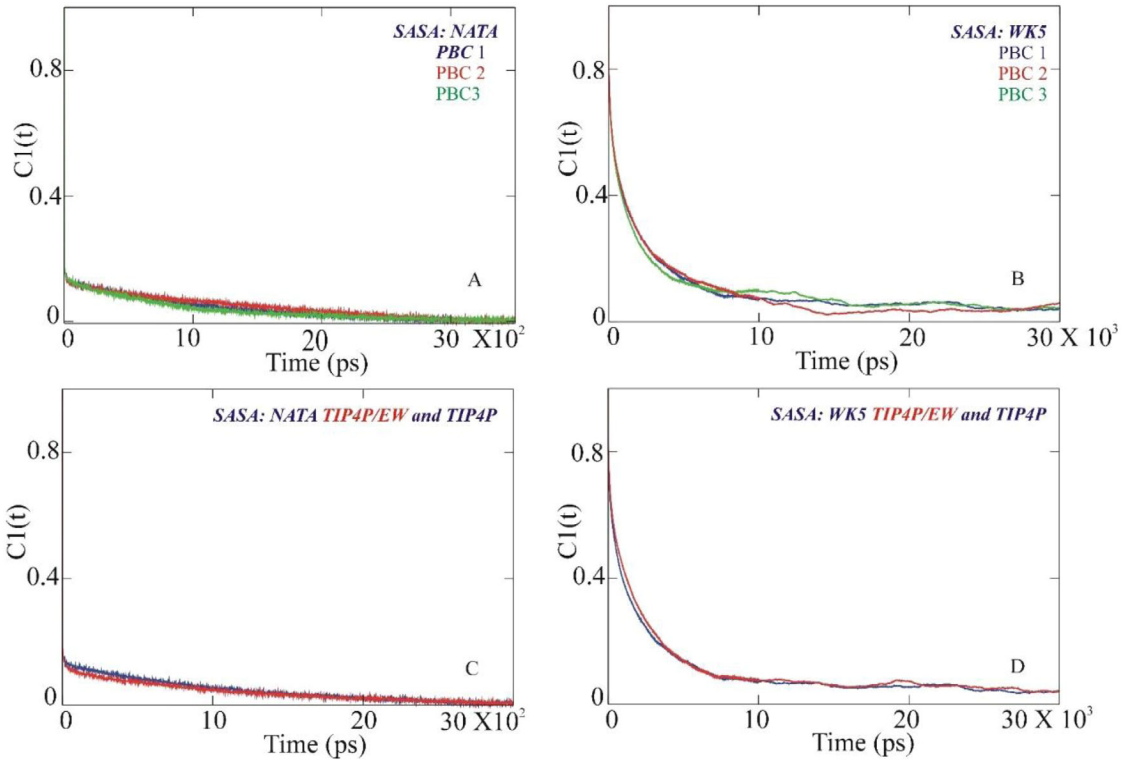

Figure 8. ACFs C1(t) for fluctuations of peptide solvent accessible surface area (SASA). (A) Different box sizes PBC1, PBC2, and PBC3 with TIP4P for NATA. (B) Different box sizes PBC1, PBC2, and PBC3 with TIP4P for WK5. (C) PBC1 box with TIP4P and TIP4P-EW for NATA. (D) PBC1 box with TIP4P and TIP4P-EW for WK5.

compares the τ_2 correlation times for the LOC and CM axes in NATA and WK5 and exhibits the same trends as discussed above. More information on axis correlation times is given in the SI.

Rotational diffusion in LOC axes

Rotational diffusion coefficients, calculated from the C_1 ACFs of three axes of the Trp indole group (described in Methods and SI), are presented in Figures 11A and C, with more

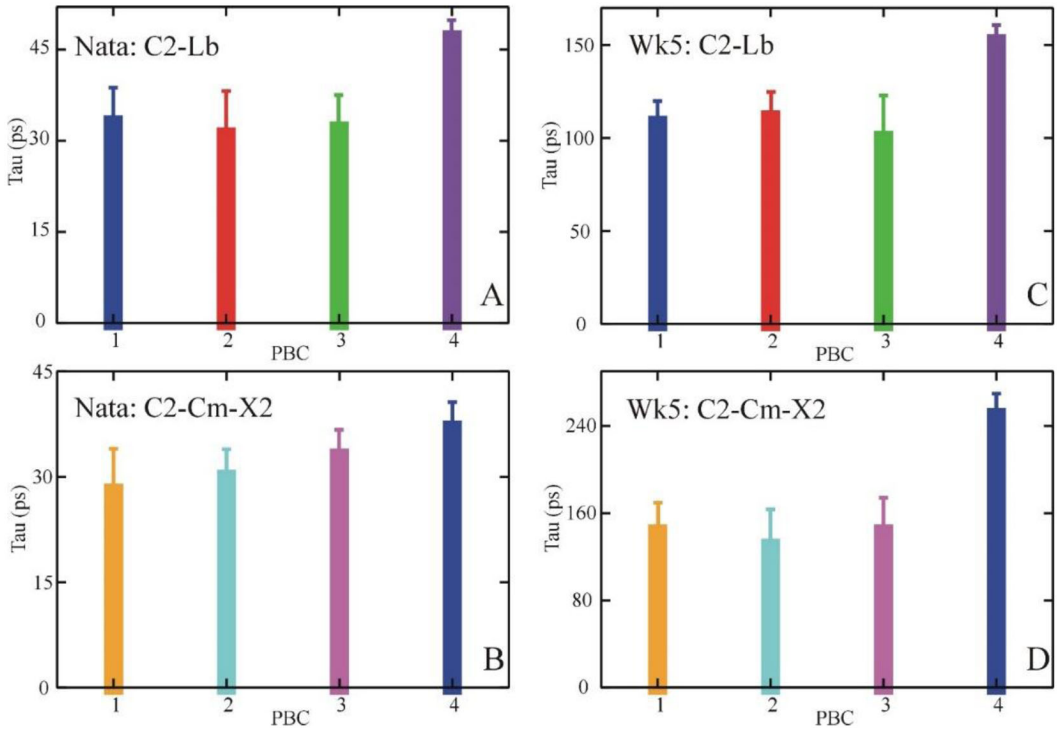

Figure 9. Rotational correlation times from $C_2(t)$ ACFs measuring time scales of peptide reorientations. Comparison of results with PBC1, PBC2, and PBC3 box sizes and TIP4P and PBC1 with TIP4PEW. (A) NATA LOC ^1L_b axis. (B) NATA CM-x2 axis. (C) WK5 LOC ^1L_b axis. (D) WK5 CM-x2 axis.

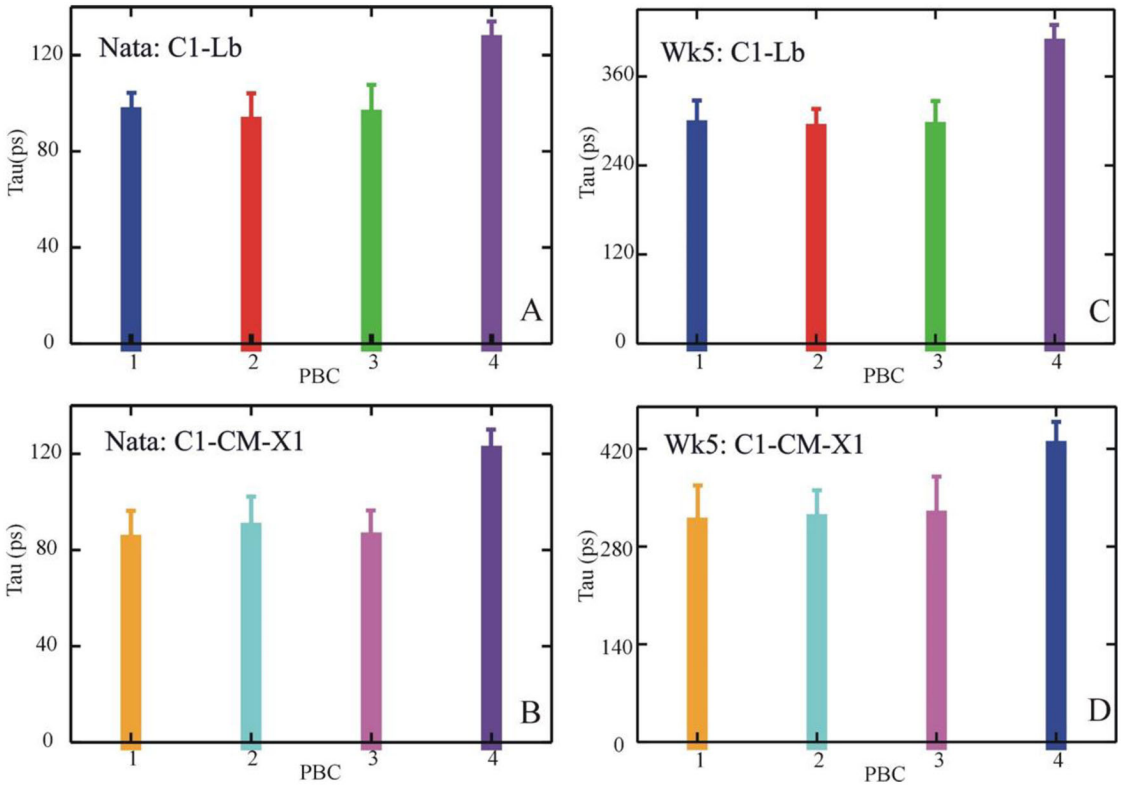

Figure 10. Rotational correlation times from $C_1(t)$ ACFs measuring time scales of peptide reorientations. Comparison of results with PBC1, PBC2, and PBC3 box sizes and TIP4P and PBC1 with TIP4PEW. (A) NATA LOC ^1L_b axis. (B) NATA CM-x1 axis. (C) WK5 LOC ^1L_b axis. (D) WK5 CM-x1 axis.

details in Supplementary Information. Besides the raw rotational diffusion coefficients D_{rot}, we also include the limiting values $D_{rot,0}$ obtained by adding corrections for the finite system size due to periodic boundary conditions, as done previously (Linke et al., 2018). The raw D_{rot} values obtained from the TIP4P MD trajectories exhibited slight variation with box size, reaching 5.99, 6.41, and 6.24 ns^{-1} for the three NATA boxes, shown in Figure 11A, and 1.78, 1.94, and 1.94 ns^{-1} for WK5, shown in Figure 11C. The NATA results all agreed within statistical errors, while for WK5, only the smallest box

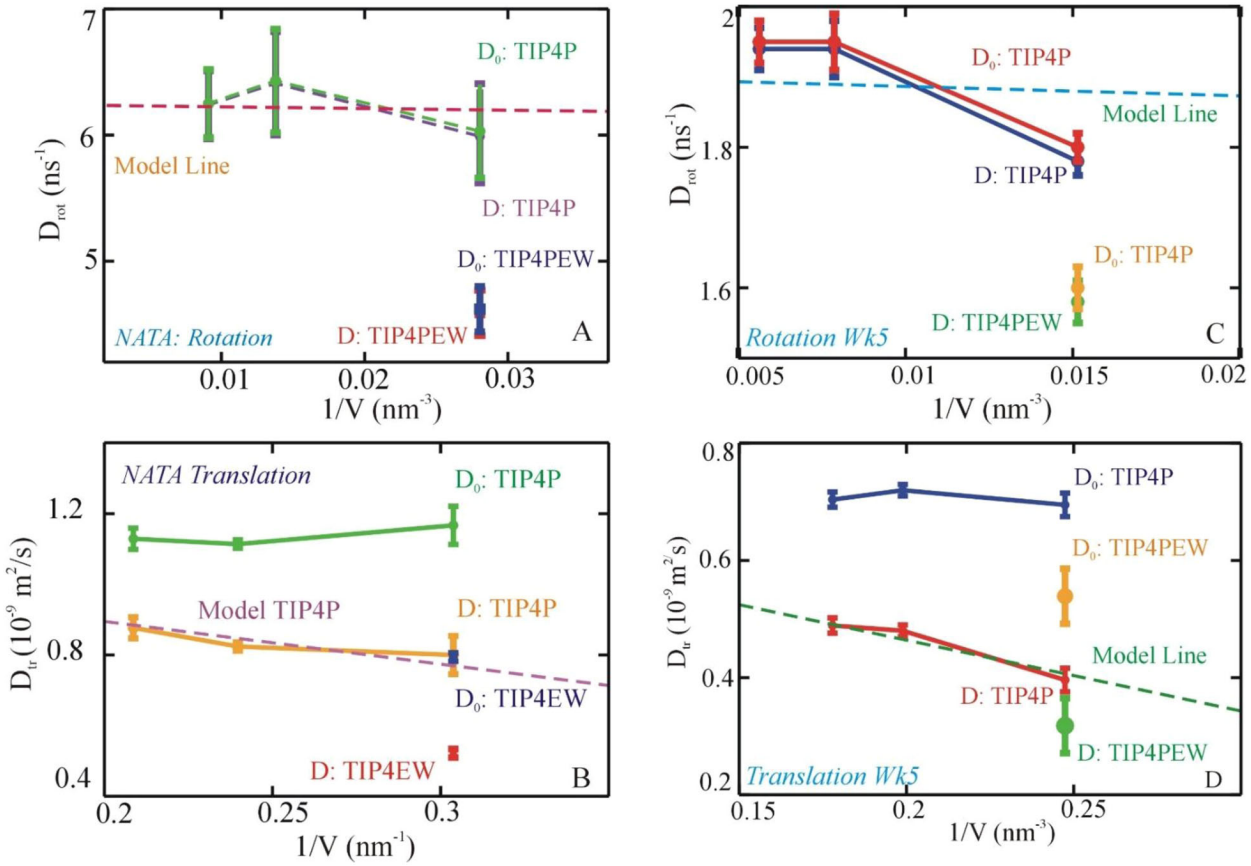

Figure 11. Peptide diffusion coefficients. (A) Rotational diffusion coefficients D_{rot} for NATA in LOC axes. Raw MD trajectory values and corrected limiting values (D_0) for three box sizes with TIP4P and one size with TIP4P. The model line represents the expected theoretical behavior of raw values in TIP4P (Jorgensen & Jenson, 1998). Raw and limiting values overlap for NATA. (B) Translational diffusion coefficients D_{tr} for NATA. Raw MD trajectory values and corrected limiting values (D_0) for three box sizes with TIP4P and one size with TIP4P. The model line represents the expected theoretical behavior of raw values in TIP4P. (C) Rotational diffusion coefficients D_{rot} for WK5 in LOC axes. Raw MD trajectory values and corrected limiting values (D_0) for three box sizes with TIP4P and one size with TIP4P. The model line represents the expected theoretical behavior of raw values in TIP4P. (D) Translational diffusion coefficients D_{tr} for WK5. Raw MD trajectory values and corrected limiting values (D_0) for three box sizes with TIP4P and one size with TIP4P. The model line represents the expected theoretical behavior of raw values in TIP4P.

results were measurably lower than those from the other two simulations. The PBC corrections were relatively small for rotational diffusion, with statistically insignificant differences between the corresponding raw D_{rot} and corrected $D_{rot,0}$ values. The raw data followed the theoretical model straight line dependence on 1/V, with V the molecular volume (Linke et al., 2018), but the line itself is almost horizontal in the data range explored by our peptides. In conclusion, PBC corrections are not crucial for small peptide rotational diffusion in boxes of a few nm in size. In the TIP4P-EW simulations, the raw rotational diffusion coefficients were 4.59 ns^{-1} for NATA and 1.38 ns^{-1} for WK5. Here, the PBC correction factors were relatively small. The decreases in diffusion rates between TIP4P-EW and TIP4P were consistent with the viscosity changes.

Rotational diffusion in CM

A detailed description of the methods and data used to calculate rotational diffusion coefficients from the C_1 ACFs of the three eigenvectors of the peptide moment of inertia tensor (CM axes), are presented in the SI. The raw D_{rot} values obtained from the TIP4P MD trajectories exhibited slight variation with box size, reaching 9.7, 8.8, and 9.1 ns^{-1} for the three NATA boxes, and 3.32, 3.26, and 3.18 ns^{-1} for WK5. These variations showed insignificant systematic trends and mostly agreed with their statistical errors, estimated as 0.4 ns^{-1} for NATA and 0.06 ns^{-1} for WK5. Similar to the LOC analysis, the PBC corrections were also relatively small, in this case. In the TIP4P/EW simulations, rotational diffusion coefficients of 6.2 for NATA and 2.4 for WK5 were calculated. The decrease in diffusion rates was due to the viscosity change between models, as expected.

Translational diffusion

Results for translational diffusion are presented in Figures 11B and D for NATA and WK5, respectively, detailed data sets are presented in SI. Besides the raw translational diffusion coefficients D_{tr}, we also include the limiting values $D_{tr,0}$ obtained by adding corrections for periodic boundary conditions, as calculated by Hummer and co-workers (Yeh & Hummer, 2004). In TIP4P water the peptide diffusion coefficient values derived from the MD trajectories were 0.800, 0.824, and 0.877×10^{-9} m^2/s for three NATA boxes, and 0.396, 0.480, and 0.489×10^{-9} m^2/s for WK5. Typical errors were in the 3-5% range. As expected, the D_{tr} data in Figures 11B and D may be fitted to a straight line as a function of *1/*

a, with *a* solvent box size (Yeh & Hummer, 2004) (the equation is in SI).

In NATA's case, the variation with box size is not statistically significant, with all three values agreeing within their errors. For WK5, the value for the smallest box size is significantly lower than the other two results. However, the translational diffusion PBC corrections were quite large, up to 45% for NATA and up to 70% for WK5. The corrected limiting values $D_{tr,0}$ obtained from the three TIP4P simulations were in agreement for each of the peptides, falling into the $1.114\text{-}1.167 \times 10^{-9}$ m^2/s range of NATA and $0.695 - 0.720 \times 10^{-9}$ m^2/s range for WK5. Generally, for small peptides in boxes of several nm sizes, it appears that it is crucial to include PBC corrections in translational diffusion analysis. For TIP4P/EW simulations, the corrected coefficients $D_{tr,0}$ were 0.794×10^{-9} m^2/s and 0.539×10^{-9} m^2/s for NATA and WK5, respectively. In this case, the PBC corrections were also significant, and the slower diffusion relative to TIP4P was in accord with the viscosity difference.

Kinetic models

Kinetic models with varying levels of trajectory discretization and kinetic coarse-graining are described in detail in the SI. We employed both Optimal Dimensionality Reduction and Markov State Modeling approaches. For NATA, the slowest kinetic process was the reorientation of the Trp χ_1 sidechain dihedral at a 1 ns time scale. Faster relaxations involved coupled transitions in backbone and sidechain dihedrals. There was no marked influence of simulation box size or water model on the kinetic modeling, either in terms of time scales or transition pathways. For WK5, the slowest process involved folding of a 3_{10} helix state from extended-type structures at a 10 ns time scale. In this pentapeptide, faster processes involved transitions between extended, PPII, and turn conformations. Kinetic models of sufficiently high resolution did not exhibit significant changes with box size or water model. To summarize the ODR results, we present the representative structures from three-dimensional kinetic models in Figures 12 and 13 for NATA and WK5, respectively.

In most cases, the MSM and ODR methods generated consistent kinetic predictions. The one exception was the MSM model for WK5 in TIP4P/EW at the highest resolution (102 dihedral clusters), which predicted the slowest relaxation at ca. 20 ns, much longer than any other MSM or ODR calculations. Details of kinetic modeling are in the SI.

Validation of simulation results

MD simulation results for NATA and WK5 were validated by examining time-resolved fluorescence anisotropy decay measurements (FAD). The time constant associated with C_2 ACFs for NATA and WK5 was compared with FAD data. Results from the FAD measurements at 303 K were used to compare with simulation results. A fit to the FAD data with a sum of two exponential functions generated two associated time constants, 5.5ps and 60ps for NATA and 26ps and 247ps for WK5. C_2 ACFs along transition dipole, ^1L_b, and Cm-X2 from molecular dynamics simulation for NATA and WK5 were compared with the FAD. A sum of two exponential fits to NATA $C_2(t)$ of ^1L_b in PBC1, PBC2, PBC3, and TIP4P-EW generated 8ps and 33ps, 1ps and 31ps, 1ps and 32ps, 3ps and 48ps, time constants, respectively. Considering NATA Cm-X2 reorientation under identical boundary conditions produced 4ps and 28ps, 5ps and 30ps, 4ps and 33ps, 3ps and 37ps, and time constants. It is important to note that time constants extracted from varying periodic boundary conditions and considering the LOC and CM axis systems produced very similar effects, with motions in TIP4P-EW slower due to the water viscosity effect. This also points out that NATA reorientation motion is barely affected by the change in periodic boundary conditions but is strongly influenced by the change in water viscosity. Reorientation along ^1L_b for WK5 C2 ACFs generated time constants of 24ps and 108ps in PBC1, 29ps and 111ps in PBC2, 19ps and 100ps in PBC2, 33ps and 152ps in TIP4P-EW. Extracted time constants associated with reorientation motion along Cm-X2 are 25ps and 143ps in PBC1, 31ps and 100ps in PBC2, 30ps and 143ps in PBC3, 45 and 250ps in EW, respectively. Time constants along ^1L_b for WK5 significantly underestimate the experimental value, 26ps, and 247ps, in all periodic boundary conditions, including the use of TIP4P-EW. This finding may be explained by the fact that both TIP4P and TIP4P-EW underestimate the shear viscosity of water (Jorgensen & Jenson, 1998,Horn et al., 2004). Cm-X2, C2(t) ACFs for WK5 underestimate the experimental time constant in PBC1, PBC2, and PBC3. Whereas in TIP4P-EW, C2(t) along Cm-X2 produced almost identical value as observed in the FAD. In summary, both NATA and WK5 MD simulations yield reorientation times that essentially do not vary with PBC box size while scaling as expected with the viscosity of the water model.

Discussion

The regulation and function of peptides and proteins are governed by the motions associated with their conformations. The reorientation dynamics are often seen as an essential component of biomolecular assembly and binding. Theoretical characterization of many experiments such as time-resolved fluorescence anisotropy (Jas et al., 2021; Jas et al., 2016), nuclear magnetic resonance (NMR) (Tjandra et al., 1995; Brüschweiler et al., 1995; Lee et al., 1997; Ghose et al., 2001; Wang et al., 1997; Boisbouvier et al., 2003; Duchardt et al., 2008), dynamic light scattering (Berne & Pecora, 2000) involves rotation. Significant effort combining theory and experiments has been employed to probe internal motions in the picosecond timescale (Shoup & Szabo, 1982; Northrup et al., 1984; Morelli & Ten Wolde, 2008; Klein & Schwarz, 2014; Ilie et al., 2014; Berne & Pecora, 2000; Woessner, 1962a; Woessner, 1962b; Lipari & Szabo, 1982; Tjandra et al., 1995; Brüschweiler et al., 1995; Lee et al., 1997; Ghose et al., 2001; Wang et al., 1997; Boisbouvier et al., 2003; Duchardt et al., 2008; Wolf et al., 2012; Debye, 1929; Perrin, 1936; Perrin, 1934; Ortega et al., 2011; McKinney et al., 2003; Boisbouvier et al., 2003). Fluorescence spectroscopy with a carefully placed fluorophore in biomolecular structure has become an essential tool to monitor dynamics and interactions

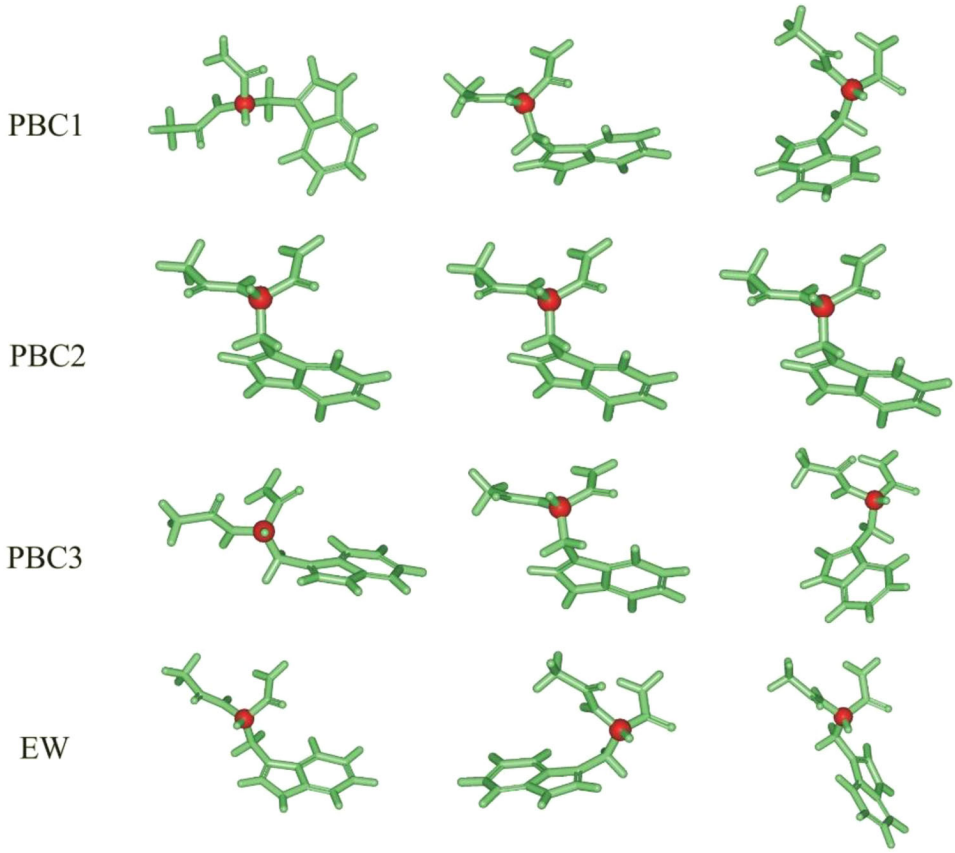

Figure 12. Representative structures for NATA ORD kinetic models with $N = 3$ aggregate states. Left-to-right: state1, state two, and state 3, described in SI. PBC1 – model with Nc = 15 and TIP4P, PBC2 – model with Nc = 16 and TIP4P, PBC3 – model with Nc = 19 and TIP4P, EW – model with Nc = 17 and TIP4P-EW. In each case, the N_c clusters are divided into $N = 3$ aggregate states. The representative structure shows the most populated cluster from each aggregate state.

(Lakowicz, 1999; Schröder et al., 2005; Loman et al., 2010; Hummer & Szabo, 2017; Szabo, 1980; Schuler et al., 2002; Margittai et al., 2003; Weiss, 1999; Schröder & Grubmüller, 2003; Munro et al., 1979; Jas et al., 2021). Time-resolved fluorescence anisotropy is used to monitor structure, conformational changes, and flexibility of the bio-molecular system in solution as the fluorophore is attached to the peptide and proteins. All-atom molecular dynamics simulation is developed into a powerful computational method to provide microscopic insight into the experimental observation. It has been suggested that the results of rotational dynamics of proteins and nucleic acid may be contaminated with finite-size effects in molecular dynamics simulation. Recent molecular dynamics study of a single domain protein and B-DNA rotational dynamics found systematic effects of solvent box size on translational and rotational diffusion upon introducing periodic boundary conditions (PBC) (Linke et al., 2018). It is of fundamental interest to examine how a significantly smaller system such as di and pentapeptides behave under different PBC by changing simulation box sizes and water models. To examine this effect, we have carried out fluorescence lifetime measurements with maximum entropy fits to characterize structural population with a lifetime stamp for two simple peptide systems NATA and WK5. We then performed time-resolved fluorescence anisotropy measurements to study reorientation dynamics for these two peptide systems. We measured fluorescence anisotropy under various conditions, such as varying temperatures and the systems' structural complexity. This experimentally measured data provided a baseline to test the validity of molecular dynamics simulations, provided the opportunity to accurately interpret the measured data, and create an atomically detailed picture with microscopic insight into the conformational dynamics. We designed and carried all-atom molecular dynamics simulations by varying the simulation box-size and water model to test the effects of finite system size on translational and rotational diffusion and internal fluctuations.

To validate simulation predictions, we have experimentally examined the time scales of FAD signals and far-UV CD spectrum at relevant temperatures for NATA and WK5. Molecular dynamics simulations in three different simulation box-size and with two different water models for NATA and WK5 were carried out to accurately interpret experimental observation and gain atomically detailed insight into the dynamical properties of the peptides in solution.

Experimental measurements and a sum of two exponential fit the FAD data yield two-time constants for NATA and WK5. Analysis of the FAD showed that the faster of the two constants remain unchanged with increasing temperature. The slower components showed significant temperature dependence, becoming faster with increasing temperature. Faster and nearly temperature-insensitive components can be attributed to the motion due to vibration upon excitation, which will then propagate and manifest as a global orientation motion. FAD analysis of NATA and WK5 showed a

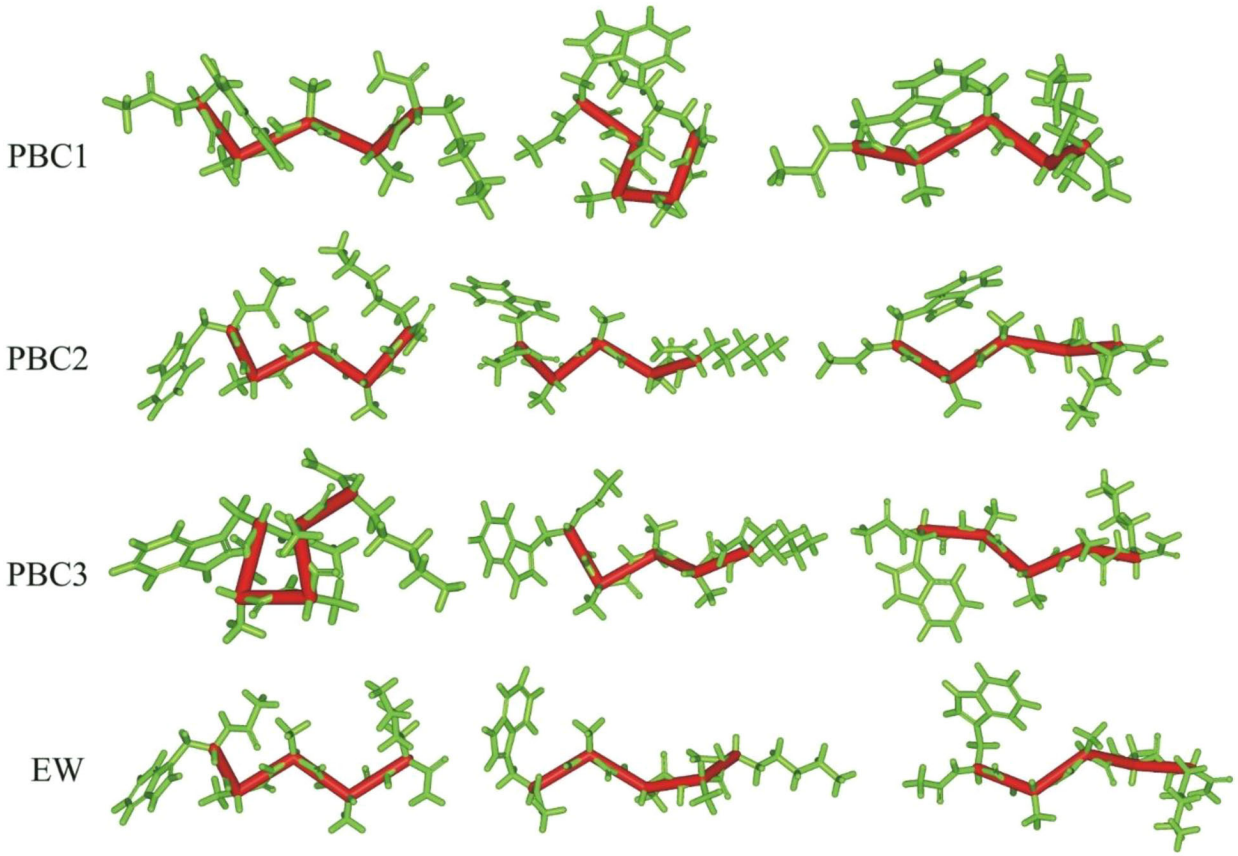

Figure 13. Representative structures for WK5 ORD kinetic models with $N = 3$ aggregate states. Left-to-right: state1, state 2, and state 3, described in SI. PBC1 – model with Nc = 31 and TIP4P, PBC2 – model with Nc = 29 and TIP4P, PBC3 – model with Nc = 35 and TIP4P, EW – model with Nc = 25 and TIP4P-EW. In each case, the N_c clusters are divided into $N = 3$ aggregate states. The representative structure shows the most populated cluster from each aggregate state.

temperature-insensitive and temperature-sensitive component for each peptide system. This observation can be inferred possibly as an initiation step, temperature-insensitive component, and a propagated motion as global reorientation (Jas et al., 2021).

Molecular dynamics simulations with three different box sizes and in two water models yielded several notable effects. The system properties examined from the MD included translational diffusion, rotational diffusion measured in a local and global axis system, and fluctuations of various structural variables. We have also analyzed the kinetic properties of peptides with ODR and MSM to study internal dynamics under different periodic boundary conditions. Notably, the internal fluctuations time scales for NATA and WK5 showed statistically insignificant variation with either solvent box size or change of water model from TIP4P to TIP4P-EW. The lack of any noticeable change with the variation of simulation box size suggests that typical minimum box sizes used in biomolecular simulations are sufficient to capture peptide conformational dynamics. An extra water molecule does not change the peptide behavior. The lack of variation with the water model indicates an absence of coupling between the internal motions of peptides and solvent in these molecules. This contrasts with the definite effects of viscosity on measured folding studies in larger systems (Linke et al., 2018). In accord with theory, translational and rotational diffusion coefficients from simulations in TIP4P and TIP4P-EW water models were approximately inversely proportional to viscosity. Thus, the global peptide motions exhibited the expected solute-solvent coupling. The detected effects of water model change on internal and external peptide dynamics are robust, with similar trends in both studied systems. However, several exciting features of the diffusion were detected, different from what is found in previous studies for larger systems (Jas et al., 2001). For both translational and rotational diffusion, the changes in rates with box size were insignificant for sizes studied here. However, the corrections for finite system size magnitudes were significant for translational diffusion coefficients D_{tr} and insignificant for rotational diffusion coefficients D_{rot}. Therefore, finite-size corrections to D_{tr} should be widely applicable in molecular dynamics simulations.

Acknowledgements

We want to acknowledge XSEDE grant TG-MCB 16009 for computer time. Parts of the simulations described were conducted at the Center for Research Computing at the University of Kansas and on computer workstations supported by the General Research Fund at the University of Kansas. We would like to thank Prof. Carey K. Johnson for allowing access to the fluorescence apparatus. GSJ would like to thank Wade Burleson and Kyle Williams for the inspirational conversation. This project was supported in part by an NSF grant, CHE1807852.

Disclosure statement

No potential conflict of interest was reported by the author(s).

ORCID

Gouri S. Jas http://orcid.org/0000-0002-0774-012X

Reference

Berne, B. J., & Pecora, R. (2000). *Dynamic light scattering: With applications to chemistry, biology, and physics*. Dover Publications. ISBN 978-1-4613-2389-1.

Boisbouvier, J., Wu, Z., Ono, A., Kainosho, M., & Bax, A. (2003). Rotational diffusion tensor of nucleic acids from 13C NMR relaxation. *Journal of Biomolecular NMR*, *27*(2), 133–142. https://doi.org/10.1023/a:1024931619957

Bowman, G. R., Pande, V. S., & Noe, F. Eds. (2014). *An introduction to Markov state models and their applications to long timescale molecular simulation*. Springer. ISBN 978-94-007-7606-7

Brooks, B. R., Brooks, C. L., Mackerell, A. D., Nilsson, L., Petrella, R. J., Roux, B., Won, Y., Archontis, G., Bartels, C., Boresch, S., Caflisch, A., Caves, L., Cui, Q., Dinner, A. R., Feig, M., Fischer, S., Gao, J., Hodoscek, M., Im, W., … Karplus, M. (2009). CHARMM: The biomolecular simulation program. *Journal of Computational Chemistry*, *30* (10), 1545–1614. https://doi.org/10.1002/jcc.21287

Brüschweiler, R., Liao, X., & Wright, P. E. (1995). Long-range motional restrictions in a multidomain zinc-finger protein from anisotropic tumbling. *Science (New York, N.Y.)*, *268* (5212), 886–889. https://doi.org/10.1126/science.7754375

Debye, P. J. W. (1929). Polar Molecules. *Angew. Chemi*, *42* (41), 995–995. https://doi.org/10.1002/ange.19290424112

Duchardt, E., Nilsson, L., & Schleucher, J. (2008). Cytosine ribose flexibility in DNA: A combined NMR 13C spin relaxation and molecular dynamics simulation study. *Nucleic Acids Research*, *36* (12), 4211–4219. https://doi.org/10.1093/nar/gkn375

Dünweg, B., & Kremer, K. (1993). Molecular dynamics simulation of a polymer chain in solution. Journal *of Chemical Physics.*, *99* (9), 6983–6997. https://doi.org/10.1063/1.465445

Ghose, R., Fushman, D., & Cowburn, D. (2001). Determination of the rotational diffusion tensor of macromolecules in solution from NMR relaxation data with a combination of exact and approximate methods-application to the determination of interdomain orientation in multidomain proteins. *Journal of Magnetic Resonance (San Diego, Calif. : 1997)*, *149* (2), 204–217. https://doi.org/10.1006/jmre.2001.2295

Hasimoto, H. (1959). On the periodic fundamental solutions of the stokes equations and their application to viscous flow past a cubic array of spheres. *Journal of Fluid Mechanics*, *5* (02), 317–328. https://doi.org/10.1017/S0022112059000222

Heinz, T. N., Van Gunsteren, W. F., & Hunenberger, P. H. (2001). Comparison of four methods to compute the dielectric permittivity of liquids from molecular dynamics simulations. Journal *of Chemical Physics.*, *115*(3), 1125–1136. https://doi.org/10.1063/1.1379764

Hess, B., Kutzner, C., van der Spoel, D., & Lindahl, E. (2008). GROMACS 4: Algorithms for highly efficient, load-balanced, and scalable molecular simulation . *Journal of Chemical Theory and Computation*, *4* (3), 435–447. https://doi.org/10.1021/ct700301q

Horn, H. W., Swope, W. C., Pitera, J. W., Madura, J. D., Dick, T. J., Hura, G. L., & Head-Gordon, T. (2004). Development of an improved four-site water model for biomolecular simulations: TIP4P-Ew. *The Journal of Chemical Physics*, *120* (20), 9665–9678. https://doi.org/10.1063/1.1683075

Hummer, G., & Szabo, A. (2015). Optimal dimensionality reduction of multistate kinetic and Markov state models. *The Journal of Physical Chemistry. B*, *119*(29), 9029–9037. 2015, https://doi.org/10.1021/jp508375q

Hummer, G., & Szabo, A. (2017). Dynamics of the orientational factor in fluorescence resonance energy transfer. *The Journal of Physical Chemistry. B*, *121* (15), 3331–3339. https://doi.org/10.1021/acs.jpcb.6b08345

Ilie, I. M., den Otter, W. K., & Briels, W. J. (2014). Rotational Brownian dynamics simulations of Clathrin cage formation. *The Journal of Chemical Physics*, *141* (6), 065101. https://doi.org/10.1063/1.4891306

Jas, G. S., Childs, E. W., & Kuczera, K. (2021). Probing coupled motions of peptides in solution with fluorescence anisotropy and molecular dynamics simulation. Chemical *Physics*, *541*, 111018. https://doi.org/10.1016/j.chemphys.2020.111018

Jas, G. S., Eaton, W. A., & Hofrichter, J. (2001). Effect of viscosity on the kinetics of α-helix and β-hairpin formation. *The Journal of Physical Chemistry B*, *105*(1), 261–272. https://doi.org/10.1021/jp0022048

Jas, G. S., Middaugh, C. R., & Kuczera, K. (2016). Probing selection mechanism of the most favorable conformation of a dipeptide in chaotropic and kosmotropic solution. *The Journal of Physical Chemistry. B*, *120* (28), 6939–6950. https://doi.org/10.1021/acs.jpcb.6b04528

Jas, G. S., Rentchler, E. C., Słowicka, A. M., Hermansen, J. R., Johnson, C. K., Middaugh, C. R., & Kuczera, K. (2016). Reorientation motion and preferential interactions of a peptide in denaturants and osmolyte. *The Journal of Physical Chemistry. B*, *120*(12), 3089–3099. https://doi.org/10.1021/acs.jpcb.6b00028

Jas, G. S., Vallejo-Calzada, R., Johnson, C. K., & Kuczera, K. (2019). Dynamic elements and kinetics: Most favorable conformations of peptides in solution with measurements and simulations. *The Journal of Chemical Physics*, *151* (22), 225102 https://doi.org/10.1063/1.5131782

Jorgensen, W. L., & Jenson, C. (1998). Temperature dependence of TIP3P, SPC and TIP4P water from NPT Monte Carlo simulations: Seeking temperatures of maximum density. *Journal of Computational Chemistry*, *19* (10), 1179–1186. https://doi.org/10.1002/(SICI)1096-987X(19980730)19:10<1179::AID-JCC6>3.0.CO;2-J

Juszczak, L. J., Zhang, Z.-Y., Wu, L., Gottfried, D. S., & Eads, D. D. (1997). Rapid Loop dynamics of Yersinia protein tyrosine phosphatases. *Biochemistry*, *36* (8), 2227–2236. https://doi.org/10.1021/bi9622130

Kaminski, G., & Jorgensen, W. L. (1996). Performance of the AMBER94, MMFF94, and OPLS-AA force fields for modeling organic liquids. *the Journal of Physical Chemistry*, *100* (46), 18010–18013. https://doi.org/10.1021/jp9624257

Klein, H. C., & Schwarz, U. S. (2014). Studying protein assembly with reversible Brownian dynamics of patchy particles. *The Journal of Chemical Physics*, *140* (18), 184112 https://doi.org/10.1063/1.4873708

Kube, S., & Weber, M. A. (2007). Coarse Graining method for the identification of transition rates between molecular conformations. *The Journal of Chemical Physics*, *126*(2), 024103. https://doi.org/10.1063/1.2404953

Lakowicz, J. R. (1999). *Principles of flourescence spectroscopy*. Springer. ISBN 978-0-387-46312-4

Lee, L. K., Rance, M., Chazin, W. J., & Palmer, A. G. III (1997). Rotational diffusion anisotropy of proteins from simultaneous analysis of 15n and 13cα nuclear spin relaxation. *Journal of Biomolecular NMR*, *9*(3), 287–298. – https://doi.org/10.1023/A:1018631009583

Li, P., Roberts, B. P., Chakravorty, D. K., & Merz, K. M. Jr. (2013). Rational design of particle mesh Ewald compatible Lennard-Jones parameters for +2 metal cations in explicit solvent. *Journal of Chemical Theory and Computation*, *9*(6), 2733–2748. 2013, https://doi.org/10.1021/ct400146w

Linke, M., Köfinger, J., & Hummer, G. (2018). Rotational diffusion depends on box size in molecular dynamics simulations. *The Journal of Physical Chemistry Letters*, *9* (11), 2874–2878. https://doi.org/10.1021/acs.jpclett.8b01090

Lipari, G., & Szabo, A. (1982). Model-free approach to the interpretation of nuclear magnetic resonance relaxation in macromolecules. 1. Theory and range of validity. *Journal of the American Chemical Society*, *104* (17), 4546–4559. https://doi.org/10.1021/ja00381a009

Loman, A., Gregor, I., Stutz, C., Mund, M., & Enderlein, J. (2010). Measuring rotational diffusion of macromolecules by fluorescence correlation spectroscopy. *Photochemical & Photobiological Sciences : Official Journal of the European Photochemistry Association and the European Society for Photobiology*, *9* (5), 627–636. https://doi.org/10.1039/b9pp00029a

Margittai, M., Widengren, J., Schweinberger, E., Schröder, G. F., Felekyan, S., Haustein, E., KöNig, M., Fasshauer, D., GrubmüLler, H., Jahn, R., & Seidel, C. A. M. (2003). Single-molecule fluorescence resonance energy transfer reveals a dynamic equilibrium between closed and open conformations of syntaxin 1. *Proceedings of the National Academy of*

Sciences of the United States of America, *100* (26), 15516–15521. https://doi.org/10.1073/pnas.2331232100

McKinney, S. A., DéClais, A.-C., Lilley, D. M. J., & Ha, T. (2003). Structural dynamics of individual Holliday junctions. *Nature Structural Biology*, ***10***(2), 93–97. https://doi.org/10.1038/nsb883

Morelli, M. J., & Ten Wolde, P. R. (2008). Reaction Brownian dynamics and the effect of spatial fluctuations on the gain of a push-pull network. *The Journal of Chemical Physics*, *129* (5), 054112 https://doi.org/10.1063/1.2958287

Munro, I., Pecht, I., & Stryer, L. (1979). Subnanosecond motions of tryptophan residues in proteins. *Proceedings of the National Academy of Sciences of the United States of America*, *76* (1), 56–60. https://doi.org/10.1073/pnas.76.1.56

Northrup, S. H., Allison, S. A., & McCammon, J. A. (1984). Brownian dynamics simulation of diffusion-influenced biomolecular reactions. Journal *of Chemical Physics*, *80* (4), 1517–1524. https://doi.org/10.1063/1.446900

Ortega, A., Amoros, D., & Garcia De La Torre, J. (2011). Prediction of hydrodynamic and other solution properties of rigid proteins from atomic- and residue-level models. *Biophysical Journal*, *101* (4), 892–898. https://doi.org/10.1016/j.bpj.2011.06.046

Perrin, F. (1934). Mouvement Brownien d'un Ellipsoide - I. Dispersion Dielectrique pour des Mole ´ cules Ellipsoidales. ´ *Journal de Physique et le Radium*, *5* (10), 497–511. https://doi.org/10.1051/jphysrad:01934005010049700

Perrin, F. (1936). Mouvement Brownien d'un ellipsoide (II). (1936) rotation libre et depolarisation des fluorescences. Translation et diffusion de ´ molecules ellipsoidales. *Journal de Physique et le Radium*, *7*(1), 1–11. — https://doi.org/10.1051/jphysrad:01936007010100

Schröder, G. F., & Grubmüller, H. (2003). Maximum likelihood trajectories from single molecule fluorescence resonance energy transfer. Journal *of Chemical Physics.*, *119* (18), 9920. https://doi.org/10.1063/1.1616511

Schröder, G. F., Alexiev, U., & Grubmüller, H. (2005). Simulation of fluorescence anisotropy experiments: probing protein dynamics. *Biophysical Journal*, *89* (6), 3757–3770. https://doi.org/10.1529/biophysj.105.069500

Schuler, B., Lipman, A., & Eaton, W. A. (2002). Probing the free-energy surface for protein folding with single-molecule fluorescence spectroscopy. *Nature*, *419* (6908), 743–747. https://doi.org/10.1038/nature01060

Senne, M., Trendelkamp-Schroer, B., Mey, A. S. J. S., Schütte, C., & Noé, F. (2012). EMMA: A software package for Markov model building and analysis. *Journal of Chemical Theory and Computation*, *8* (7), 2223–2238. https://doi.org/10.1021/ct300274u

Shoup, D., & Szabo, A. (1982). Role of diffusion in ligand binding to macromolecules and cell-bound receptors. *Biophysical Journal*, *40* (1), 33–39. https://doi.org/10.1016/S0006-3495(82)84455-X

Szabo, A. (1980). Theory of polarized fluorescent emission in uniaxial liquid crystals. Journal *of Chemical Physics.*, *72* (8), 4620–4626. https://doi.org/10.1063/1.439704

Tjandra, N., Feller, S. E., Pastor, R. W., & Bax, A. (1995). Rotational diffusion anisotropy of human ubiquitin FROM NMR relaxation. *Journal of the American Chemical Society*, *117* (50), 12562–12566. https://doi.org/10.1021/ja00155a020

Venable, R. M., Ingólfsson, H. I., Lerner, M. G., Perrin, B. S., Camley, B. A., Marrink, S. J., Brown, F. L. H., & Pastor, R. W. (2017). Lipid and peptide diffusion in bilayers: The Saffman-Delbrück model and periodic boundary conditions. *The Journal of Physical Chemistry. B*, *121* (15), 3443–3457. https://doi.org/10.1021/acs.jpcb.6b09111

Vögele, M., & Hummer, G. (2016). Divergent diffusion coefficients in simulations of fluids and lipid membranes. *The Journal of Physical Chemistry. B*, *120* (33), 8722–8732. https://doi.org/10.1021/acs.jpcb.6b05102

Wang, D., Kreutzer, U., Chung, Y., & Jue, T. (1997). Myoglobin and hemoglobin rotational diffusion in the cell. *Biophysical Journal*, *73* (5), 2764–2770. https://doi.org/10.1016/S0006-3495(97)78305-X

Weiss, S. (1999). Fluorescence spectroscopy of single biomolecules. *Science (New York, N.Y.)*, *283* (5408), 1676–1683. 2. https://doi.org/10.1126/science.283.5408.1676

Woessner, D. E. (1962a). Nuclear spin relaxation in ellipsoids undergoing rotational Brownian motion. Journal *of Chemical Physics.*, *37* (3), 647–654. https://doi.org/10.1063/1.1701390

Woessner, D. E. (1962b). Spin relaxation processes in a two-proton system undergoing anisotropic reorientation. Journal *of Chemical Physics.*, *36* (1), 1–4. https://doi.org/10.1063/1.1732274

Wolf, M., Gulich, R., Lunkenheimer, P., & Loidl, A. (2012). Relaxation dynamics of a protein solution investigated by dielectric spectroscopy. *Biochimica et Biophysica Acta*, *1824* (5), 723–730. https://doi.org/10.1016/j.bbapap.2012.02.008

Yamamoto, Y., & Tanaka, J. (1972). Polarized absorption spectra of indole and its related compounds. *Bulletin of the Chemical Society of Japan*, *45* (5), 1362–1366. https://doi.org/10.1246/bcsj.45.1362

Yeh, I.-C., & Hummer, G. (2004). System-Size dependence of diffusion coefficients and viscosities from molecular dynamics simulations with periodic boundary conditions. *The Journal of Physical Chemistry B*, *108* (40), 15873–15879. https://doi.org/10.1021/jp0477147